Theoretical analysis of square surface plasmon-polariton waveguides for long-range polarization-independent waveguiding

Jesper Jung,* Thomas Søndergaard, and Sergey I. Bozhevolnyi
Department of Physics and Nanotechnology, Aalborg University, Skjernvej 4A, DK-9220 Aalborg Øst, Denmark
(Received 8 March 2007; revised manuscript received 20 April 2007; published 26 July 2007)

Bound electromagnetic modes supported by a square metal rod embedded in a lossless dielectric medium are determined and characterized. Based on the symmetry of the waveguide configuration, a schematic overview of the supported fundamental modes is given. These fundamental modes are related to coupling between four corner modes associated with individual metal corners of the square rod waveguide. Utilizing the finite element method a numerical analysis of the waveguide is performed at telecom wavelengths (~1550 nm). The mode dispersion with the rod size, mode field orientations, profiles, and widths are presented. Unlike thin metal stripe waveguides, the square metal waveguide is shown to support long-range surface plasmon-polariton modes for both polarizations. The configuration studied is a gold core embedded in a polymer (benzocyclobutene). Surface plasmon-polariton modes of both polarizations are shown to be guided with a propagation length of approximately 3 mm for a metal core size of 200×200 nm^2. The possibility of long-range polarization-independent transmission of surface plasmon-polariton modes makes the square surface plasmon-polariton waveguide unique and a promising optical component, from which future plasmonic interconnects and circuits can benefit.

DOI: 10.1103/PhysRevB.76.035434 PACS number(s): 42.79.Gn, 42.25.Ja, 71.36.+c, 73.20.Mf

I. INTRODUCTION

The ability to transmit or direct optical signals along waveguide structures of subwavelength dimensions is crucial for the further development of integrated optics in the context of ever increasing demands for miniaturization. One way of achieving subwavelength confinement of light is by means of surface electromagnetic waves, known as surface plasmon polaritons (SPPs), propagating along an interface between a metal and a dielectric medium.[1] Over the last two decades, the research and development of different SPP waveguide configurations have considerably intensified. One of the most promising configurations studied recently, with integrated optics in mind, is a thin metal stripe (its width being much larger than its thickness) embedded in a dielectric.[2–5] This waveguide configuration offers the possibility of the mode confinement to match that of a single-mode fiber and its propagation length to extend into the millimeter range. There is, however, an important drawback, which is common for most SPP waveguide configurations, that the long-range propagation is supported only for one polarization of the electric field. A plasmonic waveguide allowing for long-range propagation of both polarizations would be a major advance in plasmonic integrated optics.

The main component of the SPP electric field is oriented perpendicular to the metal surface (due to the boundary conditions), implying thereby that when searching for the polarization-independent guiding of SPP modes, one should look at metal structures with symmetric cross sections. Indeed, experimental studies by Leosson *et al.*[6] have recently verified long-range SPP guiding along square metal rods for both polarizations. At telecom wavelengths, optical radiation was shown to propagate up to several millimeters. In this paper, the surface electromagnetic modes of square surface plasmon-polariton waveguides (SSPPWs) are determined and characterized at telecom wavelengths (~1550 nm) by means of the finite element method.[7,8] To some extent, SSPPWs have been studied theoretically by the method of lines.[9] The finite element method is known as a successful numerical technique for analyzing optical waveguide structures and has previously been utilized to characterize SPP modes in metal-clad optical waveguides[10] and to analyze gain assisted SPPs in metal slab and stripe geometries.[11]

This paper is organized as follows. In Sec. II, the waveguide structure, the SPP modes supported by the structure, and the numerical technique used in the analysis are presented. The numerical results are presented in Sec. III. The electromagnetic modes supported by a SSPPW are characterized from sub- to suprawavelength metal core sizes. The mode dispersion with the size, field orientations, and field profiles, including mode width, are presented. Lastly, the electromagnetic modes supported by the square waveguide configuration are related to the modes supported by the rectangular metal stripe configuration. Section IV presents the conclusion.

II. STRUCTURE AND NUMERICAL TECHNIQUE

A. Structure

The waveguide structure studied consists of two regions Ω and Γ. Ω is a lossy metal core with thickness t and width w. The metal core is surrounded by Γ, which is an infinite lossless dielectric material [Fig. 1(a)]. The direction of propagation is along the z axis, which is out of the paper. The metal is characterized by a complex dielectric constant ϵ_Ω, whereas the dielectric constant of the surrounding medium ϵ_Γ is real. If the width and the thickness of the metal core are identical, $t=w$, the waveguide structure is a SSPPW.

The formation of super SPP modes supported by thin metal films (metal slabs), which exhibit dispersion with film thickness, can be explained by mode coupling, due to field

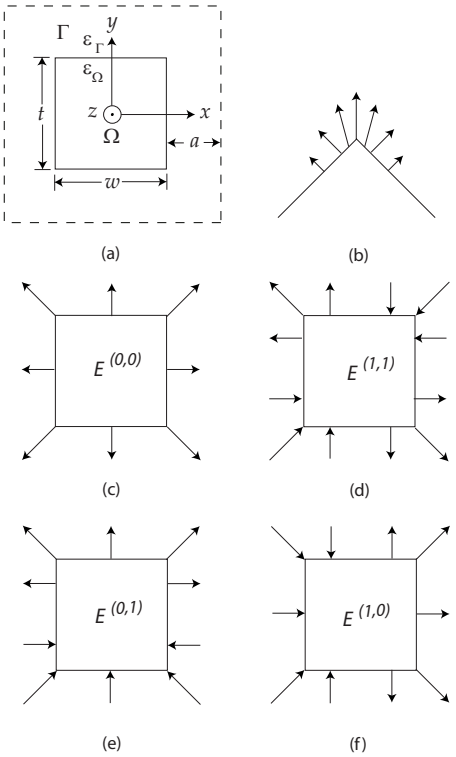

FIG. 1. (a) The waveguide structure. A lossy metal core with dielectric constant ϵ_Ω, thickness t, and width w is surrounded by a lossless dielectric material with dielectric constant ϵ_Γ. The direction of propagation is along the z axis. a is the distance between the metal-dielectric interface and the border of the computational window indicated by the outer dashed square. (b) Field orientation profile of the fundamental plasmon polariton mode supported by a single isolated corner. (c)–(f) Field orientation profiles of the possible fundamental SPP modes supported by the SSPPW configuration. The naming of the modes is according to the nomenclature described.

tunneling through the metal film, between the SPP modes guided by the two interfaces as the film becomes thin enough. In a similar way, the fundamental SPP modes supported by the SSPPW can be explained by a mode coupling of wedge or corner plasmon polariton (PP) modes supported by isolated corners [Fig. 1(b)]. Wedge modes of single isolated corners have been analyzed before.[12–16] The SSPPW configuration consists of four corners connected by four planar surfaces. One approach for determining the SPP modes supported by the SSPPW is to construct the super modes from proper combinations of the four corner modes, taking into account the symmetries of the SSPPW. As an isolated corner supports one fundamental corner mode, it is expected that the SSPPW with four corners at least supports four SPP modes. These four SPP modes will be referred to as the fundamental modes of the SSPPW. If the metal core is optically large, the four corners are far apart and there is no coupling between the four isolated corner modes. Furthermore, side modes where SPPs are propagating along each of the four planar surfaces are supported. These modes are almost zero at the corners and are localized along the sides of the metal core. Such side modes, both leaky and bound, have been analyzed for air-exposed metal stripes on glass substrates by Zia *et al.*[17] For optically large metal cores, the four fundamental modes are practically degenerate and have the mode index of a PP of a single isolated corner. As the size of the metal core decreases, the mode fields of the four corner modes start to overlap, and the degeneracy of the four fundamental modes is lifted. New modes are formed from the coupling between the four corner modes. By choosing one or the other sign (+ or −) for each corner mode, four linearly independent field combinations can be constructed (Fig. 1). The four super SPP modes are constructed from combinations of the four PP corner modes involving zero or two negative signs. Combinations with one or three negative signs are inconsistent with the overall symmetry of the system. The super modes must be symmetric or antisymmetric with respect to the x and y axes. The fundamental SPP modes supported by the SSPPW are labeled in terms of two indices. The first and second indices denote the number of nodes or sign changes in the dominant component of the electric field along the x and y axes, respectively (the y component along the x axis and the x component along the y axis). These two indices are appended as superscripts to the symbol E for the electric field. The $E^{(0,0)}$ mode [Fig. 1(c)] and the $E^{(1,1)}$ mode [Fig. 1(d)] remain unchanged after a 90° rotation around the z axis (except for a sign change in the $E^{(1,1)}$ mode). The two last modes, $E^{(0,1)}$ [Fig. 1(e)] and $E^{(1,0)}$ [Fig. 1(f)], transform into one another by a 90° rotation around the z axis. Because the square geometry of the SSPPW makes the x and the y axes interchangeable, it is evident that $E^{(0,1)}$ and $E^{(1,0)}$ are degenerate, and there is a 90° rotational symmetry around the z axis in the sum of the norm squared of $E^{(0,1)}$ and $E^{(1,0)}$. Note that it is possible to construct corner fields located on each of the four corners from a superposition of the fields of the four fundamental SSPPW modes depicted in Figs. 1(c)–1(f). Some of the super modes of the SSPPW can, in a simple manner, be related to the two super SPP modes of a thin metal film. If a metal rod is transformed into a thin and infinitely wide metal stripe, the field orientation of the $E^{(0,0)}$ mode [Fig. 1(c)] becomes similar to the field orientation of the short-range super SPP mode of a thin metal film. At the same time, the field orientation of the $E^{(0,1)}$ mode [Fig. 1(e)] becomes similar to the field orientation of the long-range SPP mode of a thin metal film. Hence, the $E^{(0,1)}$ and $E^{(1,0)}$ modes (due to the 90° rotational symmetry) can be seen as the SSPPW analogs of the long-range SPP mode of a thin metal film, while the $E^{(0,0)}$ mode can be seen as the SSPPW analog of the short-range SPP mode.

In summary, a schematic overview of the four fundamental modes supported by the SSPPW can be constructed from proper combinations of field coupling between four corner modes, taking into account the symmetries of the square waveguide structure. However, detailed information on mode dispersion, field orientation, and distribution can only be obtained from a numerical analysis of the waveguide.

It should be noted that the SPP modes of the SSPPW studied in this paper can be excited by means of end-fire or butt coupling, in which a SPP mode is excited by focusing light onto the end face of the waveguide [light incidence is along the z axis in Fig. 1(a)]. An efficient excitation can be achieved by matching the incident light field distribution (in the xy plane) to that of the SPP mode. It is thereby clear

(from symmetry considerations) that when conveniently using a linearly polarized mode of a single-mode fiber for the SSPPW excitation, only long-range $E^{(0,1)}$ and/or $E^{(1,0)}$ modes (depending on the fiber mode polarization) can be efficiently excited. The latter circumstance renders practical applications of SSPPWs for optical interconnects and integrated circuits.

B. Numerical technique

The starting point of the numerical analysis of the waveguide is the wave equation of the electric field

$$\nabla \times \nabla \times \mathbf{E} - k_0^2 \epsilon_r \mathbf{E} = 0, \tag{1}$$

where $k_0 = \omega\sqrt{\epsilon_0 \mu_0}$ is the vacuum wave number and ϵ_r is the relative dielectric constant. The solutions are sought of the form

$$\mathbf{E}(x,y,z,t) = \mathbf{E}(x,y)e^{j(\beta z - \omega t)}, \tag{2}$$

where β is the (complex) phase or propagation constant.

In order to perform a finite element analysis of the waveguide structure, the infinite dielectric medium that surrounds the metal core must be truncated. This is done by placing a square computational window that surrounds enough of the waveguide, metal core, and surrounding dielectric medium for the mode field to be negligible at the computational window boundary [dashed curve in Fig. 1(a)]. The boundary of the computational window is considered as an electric wall with $\mathbf{n} \times \mathbf{E} = 0$. It is important that the distance between the metal surface and the computational window a [see Fig. 1(a)] is large in order to prevent the size of the computational window from influencing the result of the calculation. For bounded SPP modes, the mode field must be close to zero at the boundary of the computational window. The minimum size of the computational window is directly related to the SPP mode confinement. If the SPP mode is loosely confined to the metal core, the computational window must be large compared to the size of the core. Using the finite element method, the domain within the computational window is dizcretized in a mesh of small finite triangular elements. In all calculations, the number of finite elements is increased until convergence of the phase constant is reached. The number of elements necessary to reach convergence is dependent on both the size of the metal core and the confinement of the SPP mode and changes from 15.000 to 50.000. If the mode confinement is weak, the field stretches out in the dielectric medium, and more elements are often needed to achieve convergence. The mesh of the finite elements is constructed such that the concentration of elements are high in subregions where the field distribution varies rapidly. A high concentration of elements is needed close to the metal surface and especially at the four corners. All finite element calculations are made utilizing the commercial program COMSOL MULTIPHYSICS.

III. NUMERCIAL RESULTS

In all calculations, the free space wavelength λ_0 is set to 1550 nm. This wavelength is used in optical communication because the silicon dioxide used in optical fibers has a low loss around this wavelength. The dielectric constants of the two regions are set to $\epsilon_\Omega = -131.9475 + 12.65j$[9] and $\epsilon_\Gamma = 2.356\,225$,[18] which corresponds to a gold core surrounded by a dielectric polymer of benzocyclobutene (BCB). This configuration is identical to the configuration studied experimentally by Leosson *et al.*[6] First corner rounding is briefly discussed.

TABLE I. Mode index of the fundamental corner mode vs radius of curvature calculated utilizing the finite element method.

Radius of curvature (nm)	Mode index β/k_0
2	$1.5599 + 0.0026j$
5	$1.5599 + 0.0026j$
10	$1.5591 + 0.0026j$
20	$1.5585 + 0.0025j$
50	$1.5441 + 0.0011j$

A. Corner rounding

In order to investigate the effect of corner rounding, a single isolated 90° corner [Fig. 1(b)] is analyzed for different radii of curvature by means of the finite element method. The mode index of the fundamental corner PP modes is presented in Table I. The corner mode becomes less confined and has a longer propagation length as the radius of curvature is increased. However, it is seen that if the corner rounding is below 20 nm, the effect is small. In all calculations, the corners of the metal core are rounded with a radius of curvature of 10 nm. This is mainly for numerical reasons because the field tends to become singular at sharp corners, and is furthermore justified as it is practically difficult to fabricate real structures with very sharp corners.

B. Square metal waveguide

The electromagnetic modes supported by the SSPPW are characterized for both sub- and suprawavelength sizes starting at $t = w = 200$ nm and ending at 5000 nm.

1. Mode dispersion with size

Figure 2 depicts the dispersion of the real part of the mode index [$\mathrm{Re}(\beta/k_0)$], with the size of the metal core for the electromagnetic modes supported by the SSPPW. Three of the SPP modes supported by the configuration do not have a transmission cutoff as the metal core size decreases. These modes are the $E^{(0,0)}$ mode and two degenerate modes $E^{(1,0)}$ and $E^{(0,1)}$. The last of the four fundamental modes $E^{(1,1)}$ is not supported for metal core sizes below 1500 nm. For metal cores sizes above 3000 nm, a side mode is, on the other hand, supported. As the size of the metal core decreases, the real part of the mode index of the $E^{(0,0)}$ mode increases. This corresponds to the fact that the confinement of the $E^{(0,0)}$ mode increases as the size of the metal core decreases. The real part of the mode index of two degenerate modes $E^{(1,0)}$

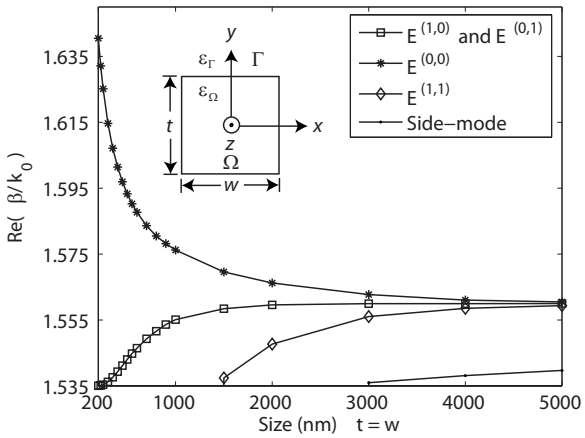

FIG. 2. The dispersion of the real part of the mode effective index of the SPP modes supported by the square waveguide with the size of the metal core.

and $E^{(0,1)}$ decreases as the size of the metal core decreases and tends asymptotically toward the refractive index of the surrounding dielectric medium. In the suprawavelength region, the four fundamental modes converge toward a four-time degenerate SPP mode with a mode index of a PP mode supported by a single isolated corner. The analysis of an isolated corner with a 10 nm radius of curvature yielded $\mathrm{Re}(\beta/k_0)=1.5591$. This value corresponds well to the value of the four fundamental modes of a SSPPW with a metal core size of 5000 nm (Fig. 2). The side mode is a mode where SPPs propagate along each of the four sides of the square metal core. The side mode has transmission cutoff for metal core sizes below approximately 3000 nm.

Figure 3 depicts the dispersion of the propagation length $L=[2\ \mathrm{Im}(\beta)]^{-1}$ with the size of the metal core. The two degenerate modes $E^{(1,0)}$ and $E^{(0,1)}$ become long range, with propagation lengths above 1 mm, when the size of the metal core is decreased below 300 nm. For a metal core size of 200 nm, the propagation length of the two degenerate modes is approximately 3 mm. 3 mm is not long range if compared to the propagation length of optical signals in standard optical fibers. However, it is long range measured in wavelengths and can be sufficient for plasmonic communication on an optical chip. The propagation length of the $E^{(0,0)}$ mode decreases as the size of the metal core decreases. If the metal core size is 200 nm, $L_{E^{(0,0)}}\approx 16$. For suprawavelength metal core sizes, the propagation lengths of the four fundamental SPP modes converge toward the propagation length of a PP mode supported by a single isolated corner with $L\approx 48\ \mu$m. The propagation length of the less confined side mode is larger than the propagation lengths of the four fundamental modes. A comparison of Figs. 2 and 3 reveals that the $E^{(1,1)}$ mode has both a lower $\mathrm{Re}(\beta/k_0)$ and a smaller propagation length than the $E^{(0,0)}$ for suprawavelength metal core sizes. This is not physically intuitive because a lower $\mathrm{Re}(\beta/k_0)$ normally implies that the mode is less confined and should therefore have a longer propagation length. This phenomenon is also observed, but not commented on, in the theoretical study of metal stripes by Berini.[2] The numerical technique utilized by Berini is the method of lines, which is another numerical approach besides the finite element method utilized in this paper. As both approaches imply the same tendency, it is not considered as an error.

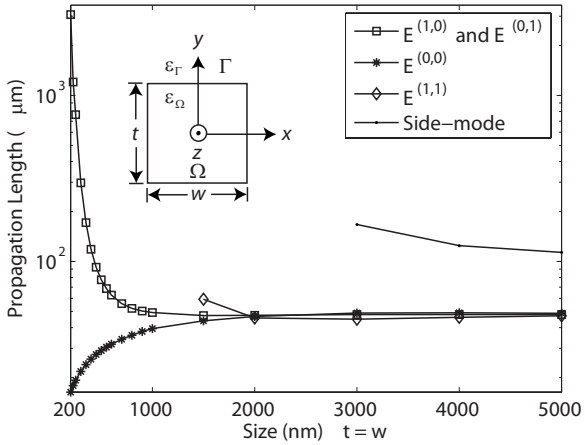

FIG. 3. The dispersion of the propagation length of the SPP modes supported by the square waveguide with the size of the metal core. The propagation length is calculated as $L=[2\ \mathrm{Im}(\beta)]^{-1}$.

The $E^{(0,0)}$ mode is the SSPPW analog of the fundamental SPP mode supported by the circular SPP waveguide, which was theoretically analyzed by Takahara *et al.*[19] With the $E^{(0,0)}$ mode, it is possible to achieve high mode confinement at the price of a high propagation loss. The $E^{(0,0)}$ mode, is therefore not suitable for plasmonic communication but could possibly be used in a SPP resonator based on slow SPP modes propagating back and forth along a thin metal wire of finite length.[20]

The $E^{(1,0)}$ and $E^{(0,1)}$ modes can be utilized for polarization-independent long-range SPP guiding. The $E^{(1,0)}$ mode is almost entirely polarized along the x axis and guides x-polarized light. The $E^{(0,1)}$ mode is polarized along the y axis and guides y-polarized light. As $E^{(1,0)}$ and $E^{(0,1)}$ are degenerate, excitation by means of end-fire or butt coupling will allow SPP guiding with the same mode index (and propagation loss) for both polarizations of the incident light. This makes the SSPPW unique because, as argued in the Introduction, metal stripe waveguides are very polarization dependent. The theoretically predicted propagation lengths of the $E^{(1,0)}$ and $E^{(0,1)}$ modes in Fig. 3 correspond well to the experimental results reported by Leosson *et al.*[6]

2. Electric field orientation in the xy plane

Arrow plots of the electric field orientation in the xy plane are presented for the four fundamental modes. The orientation of the electric field is indicated by arrows (Figs. 4–6). The length of the x (y) component of the arrow is proportional to the amplitude of the E_x (E_y) component of the electric field. The norm of the electric field is also depicted in the arrow plots. The electric field orientation of the $E^{(0,0)}$ mode (Fig. 4) has a mirror symmetry with respect to both x and y axes and is perpendicular to the metal surface along all four sides. This is in good agreement with the schematic overview of the $E^{(0,0)}$ mode presented in Fig. 1(c). Figure 5 shows how the $E^{(0,1)}$ mode has a main field polarization along the y axis. The field orientation plot of the $E^{(1,0)}$ mode is obtained by a

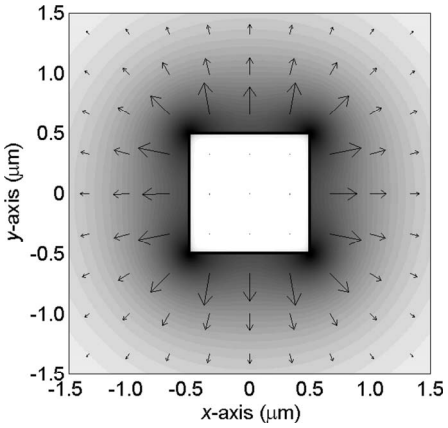

FIG. 4. Magnitude and orientation of the electric field in the xy plane of the $E^{(0,0)}$ mode for a metal core size of 1 μm.

90° rotation of the plot of the $E^{(0,1)}$ mode around the z axis. Thus, the $E^{(1,0)}$ mode has a main polarization along the x axis. The numerical results of the $E^{(0,1)}$ and $E^{(1,0)}$ modes are also in good agreement with Figs. 1(e) and 1(f). However, the numerical results show very clearly that these two degenerate modes are strongly polarized along the y and x axes, respectively. The arrow plot of the $E^{(1,1)}$ mode shows the orientation and magnitude of the electric field for a metal core size of 2 μm. This mode has a transmission cutoff for metal core sizes below approximately 1500 nm. The plot shows that the mode field (x and y components) is zero at the middle of all four sides of the metal core. As the metal core size decreases, there is not enough space along the sides to sustain these zeros, and the mode therefore has a transmission cutoff.

3. Mode width

The mode width is determined for metal core sizes below 1000 nm. The mode width $2r_w$ is defined as two times the distance from the center of the metal core to the point where the norm of the electric field has decayed to $1/e$ of its maximum value. The mode width of the $E^{(0,0)}$ is determined along the x axis. For $E^{(1,0)}$ and $E^{(0,1)}$, the mode width is determined along the x and y axes, respectively. The mode width is defined by the following equation:

$$E_{norm}(r_w) = \frac{1}{e} E_{norm}^{max}, \tag{3}$$

where E_{norm}^{max} is the maximum value of the norm of the electric field and r_w is the half of the mode width. A schematic illustration of how the mode width is estimated is depicted in the inset in Fig. 7. The mode width is illustrated by the double arrow. The solid square represents the size of the metal core. It can be seen that the skin depth of the electric field in the

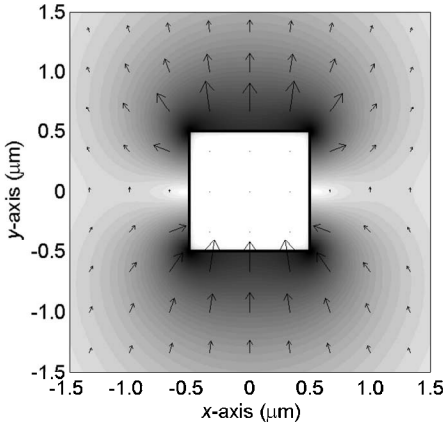

FIG. 5. Magnitude and orientation of the electric field in the xy plane of the $E^{(0,1)}$ mode for a metal core size of 1 μm. The field orientation plot of the $E^{(1,0)}$ mode is obtained by a counterclockwise rotation of 90° around the z axis, which is out of the paper.

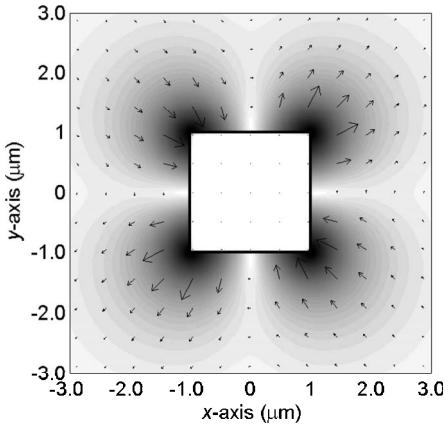

FIG. 6. Magnitude and orientation of the electric field in the xy plane of the $E^{(1,1)}$ mode for a metal core size of 2 μm.

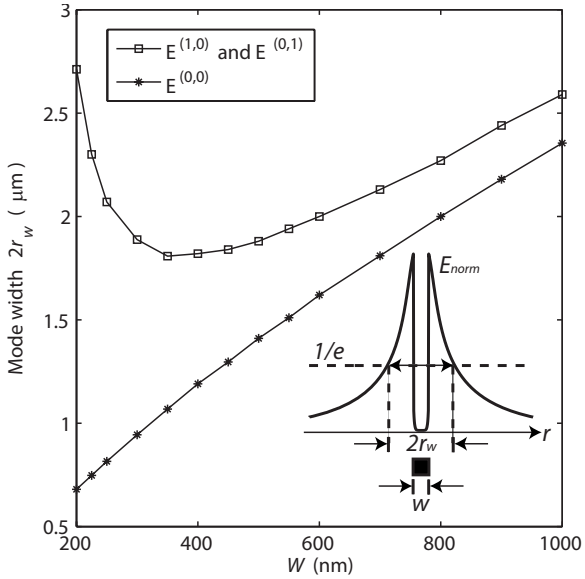

FIG. 7. Mode width versus metal core size for the $E^{(1,0)}$, $E^{(0,1)}$, and $E^{(0,0)}$ modes for metal core sizes below 1000 nm. The inset shows schematically how the mode width $2r_w$ is defined. The solid line represents the norm of the electric field along the axis by which the mode width is determined, and the dashed line is $1/e$ of the maximum of the norm of the electric field. The size of the metal core is indicated by the black square.

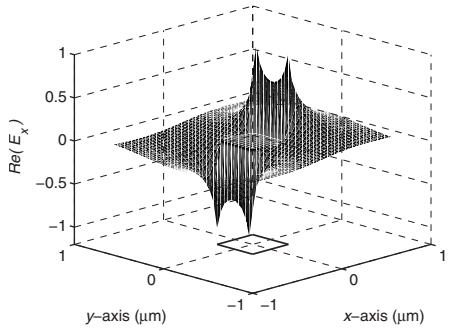

(a) $\mathrm{Re}(E_x)$ of the $E^{(0,0)}$ mode.

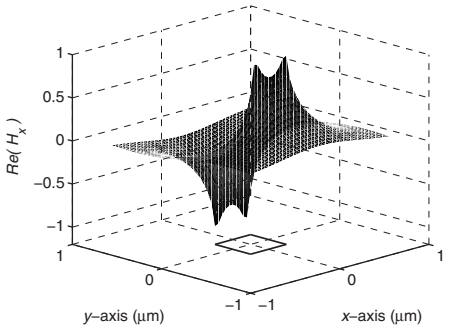

(b) $\mathrm{Re}(H_x)$ of the $E^{(0,0)}$ mode.

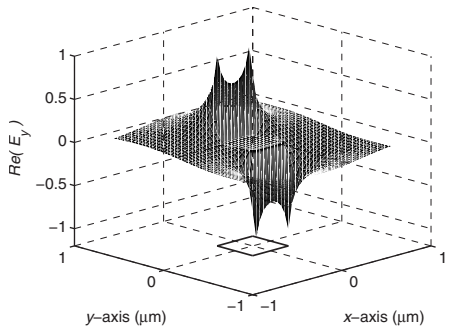

(c) $\mathrm{Re}(E_y)$ of the $E^{(0,0)}$ mode.

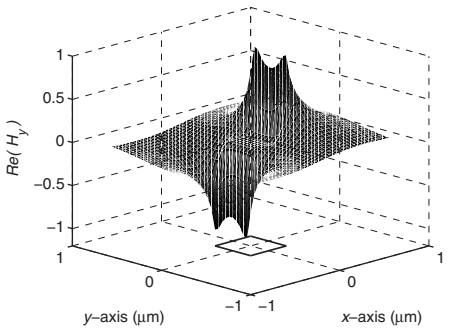

(d) $\mathrm{Re}(H_y)$ of the $E^{(0,0)}$ mode.

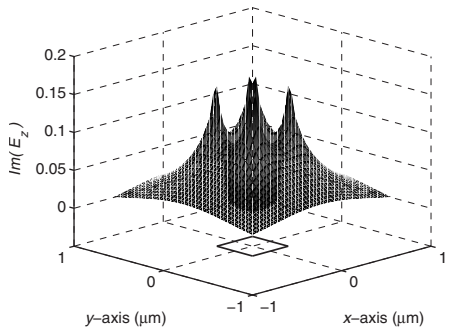

(e) $\mathrm{Im}(E_z)$ of the $E^{(0,0)}$ mode.

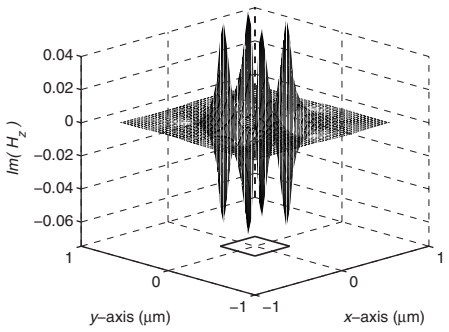

(f) $\mathrm{Im}(H_z)$ of the $E^{(0,0)}$ mode.

FIG. 8. Field distribution profiles of the electric and magnetic field components of the $E^{(0,0)}$ mode over a cross section of the waveguide for a metal core size of 400 nm. The electric and magnetic field components are normalized by $\max(|E_y|)=1$ and $\max(|H_x|)=1$.

metal is very small and that the electric field decays in an exponential manner in the dielectric. The mode width versus metal core size of the two degenerate modes $E^{(1,0)}$ and $E^{(0,1)}$ (Fig. 7) shows that the mode width increases rapidly when the metal core decreases below 300 nm. This indicates that the $E^{(1,0)}$ and $E^{(0,1)}$ modes are weakly confined to the metal structure when the metal core decreases below 300 nm. The mode width of the two degenerate modes has a distinct minimum at a metal core size of approximately 400 nm. Thus, the smallest mode field of the long-range modes is achieved for a metal core size of approximately 400 nm. The mode width of the $E^{(0,0)}$ mode decreases as the metal core size decreases. When the size of the metal core becomes large, the mode width of all the fundamental modes tends asymptotically toward the size of the metal core. In general, it can be seen that it is possible to tune the size of the SPP mode by choosing the right size of the metal core. From a technological point of view, this is valuable because the mode size of the SSPPW can be custom designed to match, e.g., the size of an optical fiber mode. Thus, by choosing the right size of the metal core, a good overlap with an optical fiber mode can be achieved. An optical fiber has two degenerate fundamental guided modes. In comparison, the SSPPW has four fundamental modes, but only three of them are supported for subwavelength metal core sizes. These three modes are the two degenerate long-range modes ($E^{(1,0)}$ and $E^{(0,1)}$) and the

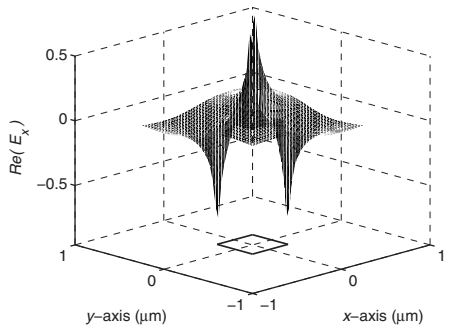

(a) Re(E_x) of the $E^{(0,1)}$ mode.

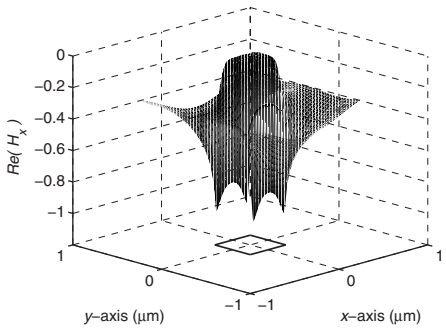

(b) Re(H_x) of the $E^{(0,1)}$ mode.

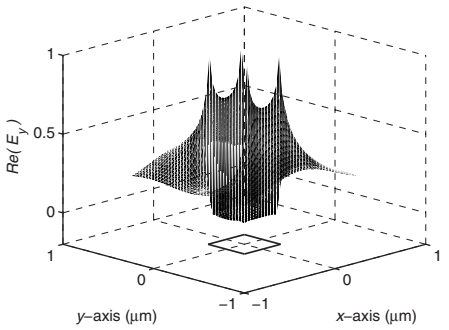

(c) Re(E_y) of the $E^{(0,1)}$ mode.

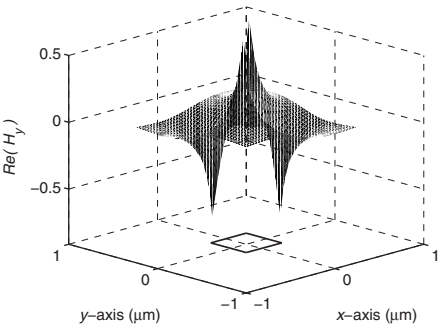

(d) Re(H_y) of the $E^{(0,1)}$ mode.

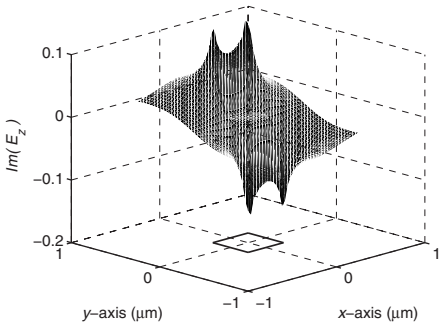

(e) Im(E_z) of the $E^{(0,1)}$ mode.

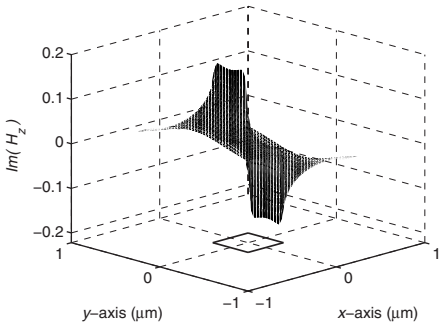

(f) Im(H_z) of the $E^{(0,1)}$ mode.

FIG. 9. Field distribution profiles of the electric and magnetic field components of the $E^{(0,1)}$ mode over a cross section of the waveguide for a metal core size of 400 nm. The electric and magnetic field components are normalized by $\max(|E_y|)=1$ and $\max(|H_x|)=1$. The field distribution of the $E^{(1,0)}$ is obtained by rotating the entire waveguide structure 90° around the z axis.

short-range mode ($E^{(0,0)}$). Regarding plasmonic communication, it is preferable to couple light from an optical fiber to the long-range modes. However, if the short-range mode is also excited, it will die out fast due to absorption. Furthermore, a good overlap between an optical fiber mode and the long-range modes will result in a poor overlap with the short-range mode because the mode size of the short-range mode is small compared to the long-range mode and because of symmetry mismatch with the optical fiber mode. This is especially pronounced for metal core sizes below approximately 400 nm. Roughness along the waveguide could, aside from scattering, also result in a continuous coupling of energy from the long-range to the short-range mode. However, in experiments, this does not seem to be a problem.[6]

4. Field distribution profiles

Field distribution profiles of the fundamental SSPPW modes are presented. All field components are, in general, complex but are presented as Re(E_x), Re(E_y), Re(H_x), Re(H_y), Im(E_z), and Im(H_z). This is chosen because the real parts of the transverse components are larger than (and equal in distribution to) the imaginary parts and because the real parts of the longitudinal components are small compared to the imaginary parts. Figure 8 shows the field distribution profiles of the six field components of the $E^{(0,0)}$ mode over a cross section of the waveguide for a metal core size of 400 nm. The electric field components are normalized such that the absolute maximum of E_y is unity. The magnetic field

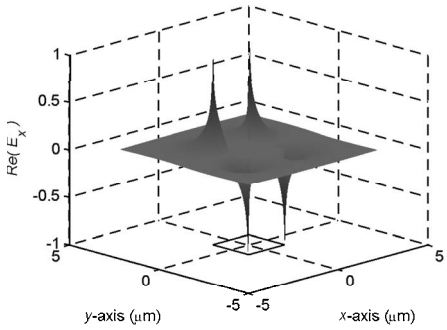

(a) Re(E_x) of the $E^{(1,1)}$ mode.

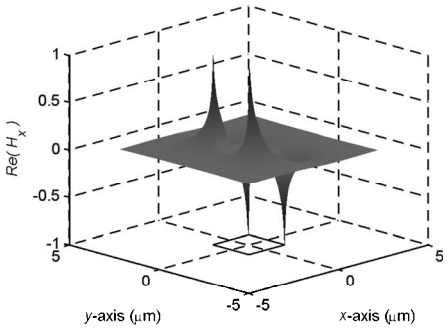

(b) Re(H_x) of the $E^{(1,1)}$ mode.

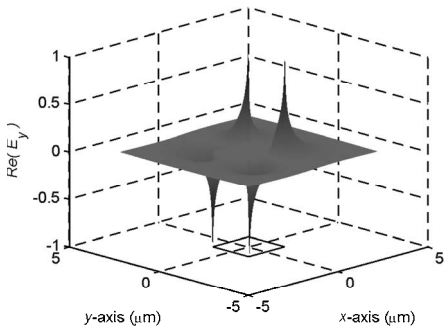

(c) Re(E_y) of the $E^{(1,1)}$ mode.

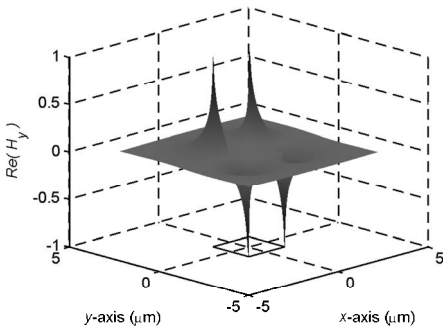

(d) Re(H_y) of the $E^{(1,1)}$ mode.

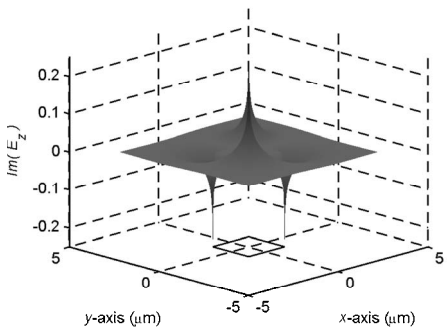

(e) Im(E_z) of the $E^{(1,1)}$ mode.

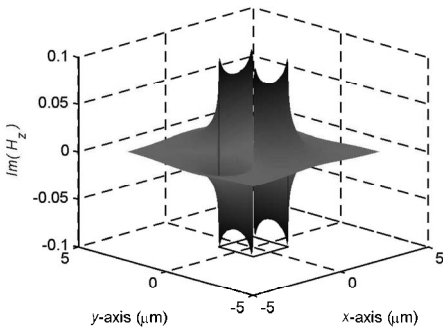

(f) Im(H_z) of the $E^{(1,1)}$ mode.

FIG. 10. Field distribution profiles of the electric and magnetic field components of the $E^{(1,1)}$ mode over a cross section of the waveguide for a metal core size of 2000 nm. The electric and magnetic field components are normalized by $\max(|E_y|)=1$ and $\max(|H_x|)=1$.

components are normalized such that the absolute maximum of H_x is unity. E_x and E_y are equal in size, and $E^{(0,0)}$ has therefore no dominating electric field component. H_x and H_y are also identical in size. The maximum of all six components are located at the corners of the metal core, and all six components decay in an exponential-like manner away from metal surfaces. Figure 9 shows the field distribution profiles of the $E^{(0,1)}$ mode. Because $E^{(1,0)}$ and $E^{(0,1)}$ are degenerate, the field distribution profiles calculated by means of the finite element method utilizing COMSOL MULTIPHYSICS are often a mixture of the two modes. In order to avoid this, it was necessary to place electric walls ($\mathbf{n}\times\mathbf{E}=0$) along the x and y axes for the $E^{(0,1)}$ and $E^{(1,0)}$ modes, respectively. The dominating electric and magnetic field components of the $E^{(0,1)}$ mode is E_y and H_x, respectively. As the SSPPW has a 90° rotational symmetry around the z axis, the field components of the $E^{(1,0)}$ mode can be directly deduced from the field components of the $E^{(0,1)}$ mode. The $E^{(1,0)}$ mode is simply the $E^{(0,1)}$ mode rotated 90° around the z axis. Utilizing this, it is readily seen that the dominating electric and magnetic field components of the $E^{(1,0)}$ mode is E_x and H_y, respectively. The guiding of both x- and y-polarized long-range SPP modes of the SSPPW is thus a direct consequence of the 90° rotational symmetry of the physical structure of the waveguide. The six electromagnetic field components of the $E^{(1,1)}$ are presented in Fig. 10. The x and y components of the

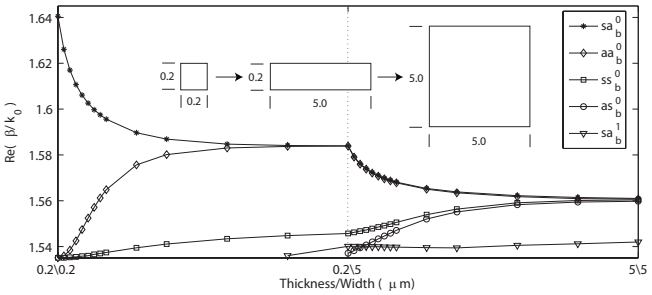

FIG. 11. The mode dispersion vs size of the structure is calculated starting from a subwavelength size SSPPW going through the rectangular waveguide and ending at a suprawavelength size SSPPW. The inset in the figure shows how the dimensions of the metal core changes during the finite element analysis. All sizes are given in micrometers.

electric field of this mode dominate equally, and the mode therefore has no dominating electric field component. This is also the case for the transverse magnetic components.

C. Rectangular vs square metal waveguides

In order to investigate how the SPP modes supported by the square metal waveguide are related to the modes supported by the rectangular metal waveguide (the metal stripe $t \ll w$), the mode dispersion is calculated starting from a subwavelength size SSPPW going through the rectangular waveguide and ending at a suprawavelength size SSPPW (Fig. 11). Starting with a SSPPW of 200 nm, the width w is increased to 5000 nm (the metal stripe structure), and subsequently the thickness t is increased to 5000 nm (see inset in Fig. 11). The four modes transforming into the corner modes of the SSPPW are in the nomenclature developed by Berini,[2] named sa_b^0, aa_b^0, ss_b^0, and as_b^0. In this nomenclature, the first two characters specify the symmetries of the dominating electric field component with respect to the y and x axes, respectively. The subscript b specifies that the mode is bound. The subscript could be l if the mode is leaky. The superscript specifies the number of extrema observed in the field distribution of the dominating electric field component along the largest transverse dimension of the metal core. As the two degenerate modes of the SSPPW have the same symmetry and number of extrema in the dominating field component, Berini introduced a second subscript[9] in order to separate the two modes from each other. The extra subscript is either x or y, which indicates that the dominating electric field component is either E_x or E_y. The four fundamental modes of the SSPPW $E^{(0,0)}$, $E^{(0,1)}$, $E^{(1,0)}$, and $E^{(1,1)}$ are with Berini's notation, named sa_b^0, ss_{bx}^0, ss_{by}^0, and as_b^0. In the metal stripe configuration, these are named sa_b^0, aa_b^0, ss_b^0, and as_b^0, respectively. For a SSPPW with a metal core size of 5000 nm, the latter four modes are practically degenerate with a mode index equal to the mode index of a PP mode supported by an isolated corner. In the SSPPW configuration, these modes are named $E^{(0,0)}$, $E^{(1,0)}$, $E^{(0,1)}$, and $E^{(1,1)}$. When the thickness is decreased, the four modes split up into two almost degenerate upper branches, sa_b^0 and aa_b^0, and into two lower branches, ss_b^0 and as_b^0. sa_b^0 and aa_b^0 are named corner modes and ss_b^0 is named the dominant symmetric stripe mode.[3] The two upper branches have an antisymmetry in the dominating electric field component across the x axis, whereas the two lower branches have a symmetry. The side mode supported by the suprawavelength size SSPPW is also supported by the metal stripe configuration and is named sa_b^1 with Berini's notation. The sa_b^1 is also named the dominant antisymmetric stripe mode.[3] When the width of the metal stripe is decreased, the degeneracy of the two upper branches are lifted and the two modes split up. When the metal core becomes square, the sa_b^0, aa_b^0, and ss_b^0 modes of the metal stripe becomes the $E^{(0,0)}$, $E^{(1,0)}$, and $E^{(0,1)}$ modes of the SSPPW, respectively. In the configuration studied here (BCB, gold, and $\lambda_0 = 1550$ nm), the as_b^0 and sa_b^1 modes have transmission cutoffs for $w \approx 5000$ nm and $w \approx 4000$ nm, respectively. The dispersion branch of the as_b^0 mode crosses the dispersion branch of the sa_b^1 mode as the thickness of the metal stripe is reduced. Such crossing is also observed in the analysis of metal stripe waveguides by Berini.[2] An investigation of the field distribution profiles of the two modes in the crossing region shows that the two modes are very different in distribution.

IV. CONCLUSION

In conclusion, we have described and characterized the surface electromagnetic modes supported by SSPPWs at telecom wavelengths (~1550 nm) for both sub- and suprawavelength metal core sizes. It was shown how mode coupling between four plasmon polariton modes of isolated corners and the symmetries of the SSPPW can be used to deduce a schematic overview of the fundamental SPP modes supported by the structure. The technique utilized for the numerical analysis of the SSPPWs was the finite element method. The configuration studied was a square gold core surrounded by an infinite lossless dielectric polymer of BCB. The mode dispersion with the size, field orientations, and field profiles, including mode width, have been presented. The SPP modes supported by the SSPPW have been related to the modes supported by the rectangular metal stripe configuration, and it was shown how three of the fundamental stripe modes transform into three of the fundamental modes of the SSPPW as the stripe is gradually changed to a SSPPW. For subwavelength metal core sizes, the three modes supported by the SSPPW are one short range and two degenerate long range. The short-range mode is the SSPPW analog of the fundamental SPP mode supported by the circular SPP waveguide.[19] With the short-range SSPPW mode, it is possible to achieve high mode confinement at the price of a significant increase in the propagation loss. The short-range mode can possibly be used in SPP resonators based on slow SPP modes propagating back and forth along a thin metal wire of finite length. The two degenerate modes become long range as the size of the metal core decreases and can be utilized for long-range SPP guiding. For a metal core size of 200 nm, the two degenerate modes have a propagation

length of approximately 3 mm. One of the long-range modes is polarized along the *x* axis, whereas the other is polarized along the *y* axis. These modes allow for polarization-independent plasmonic communication. Thus, unlike the thin metal stripe waveguides, the SSPPW supports long-range SPP waves for both polarizations. This makes the SSPPW unique and a promising optical component from which future plasmonic communication can benefit.

ACKNOWLEDGMENTS

The authors gratefully acknowledge the financial support (J.J., T.S. and S.I.B.) from the NABIIT project financed by the Danish Research Agency (Contract No. 2106-05-033), (T.S.) from the Danish Research Council for Technology and Production, and (S.I.B.) from the European Network of Excellence, Plasmo-nano-devices (FP6-2002-IST-1-507879).

*jung@physics.aau.dk

[1] H. Raether, *Surface Plasmons: On Smooth and Rough Surfaces and on Gratings*, 1st ed. (Springer-Verlag, New York, 1988).
[2] P. Berini, Phys. Rev. B **61**, 10484 (2000).
[3] S. J. Al-Bader, IEEE J. Quantum Electron. **40**, 325 (2004).
[4] P. Berini, Opt. Express **7**, 327 (2000).
[5] P. Berini, Opt. Lett. **24**, 1011 (1999).
[6] K. Leosson, T. Nikolajsen, A. Boltasseva, and S. I. Bozhevolnyi, Opt. Express **14**, 314 (2006).
[7] T. Itoh, *Numerical Techniques for Microwave and Millimeter-Wave Passive Structures*, 1st ed. (Wiley, New York, 1989).
[8] J. Jin, *The Finite Element Method in Electromagnetics*, 2nd ed. (Wiley, New York, 2002).
[9] P. Berini, U.S. Patent No. 6,741,782 (25 May 2004) (http://www.uspto.gov/).
[10] C. Themistos, B. M. A. Rahman, M. Rajarajan, K. Kalli, and K. T. V. Grattan, Appl. Opt. **45**, 8523 (2006).
[11] M. P. Nezhad, K. Tetz, and Y. Fainman, Opt. Express **12**, 4072 (2004).
[12] E. Feigenbaum and M. Orenstein, Opt. Express **14**, 8779 (2006).
[13] A. Eguiluz and A. A. Maradudin, Phys. Rev. B **14**, 5526 (1976).
[14] D. F. P. Pile, T. Ogawa, D. K. Gramotnev, T. Okamoto, M. Haraguchi, M. Fukui, and S. Matsuo, Appl. Phys. Lett. **87**, 061106 (2005).
[15] A. D. Boardman, R. Garcia-Molina, A. Gras-Marti, and E. Louis, Phys. Rev. B **32**, 6045 (1985).
[16] L. Dobrzynski and A. A. Maradudin, Phys. Rev. B **6**, 3810 (1972).
[17] R. Zia, M. D. Selker, and M. L. Brongersma, Phys. Rev. B **71**, 165431 (2005).
[18] A. Boltasseva, T. Nikolajsen, K. Leosson, K. Kjaer, M. S. Larsen, and S. I. Bozhevolnyi, J. Lightwave Technol. **23**, 413 (2005).
[19] J. Takahara, S. Yamagishi, H. Taki, A. Morimoto, and T. Kobayashi, Opt. Lett. **22**, 475 (1997).
[20] T. Søndergaard and S. I. Bozhevolnyi, Phys. Rev. B **75**, 073402 (2007).